A double vortex sheet model of the viscous flow near the trailing edge of a lifting aerofoil

A. R. Oliver*

Classical definitions of boundary layer mass and momentum flux deficiency thicknesses can lead to gross errors when applied to measurements near a trailing edge where the flow curvature in the free stream is appreciable. This paper presents a double vortex sheet model as a development from the single vortex sheet model of Helmholtz and others. Two bound vortex sheets define a potential function which can describe a flow with the same mass and momentum flux deficiencies as the viscous regions. The bound nature of these sheets allows the modelling of the integral properties of these regions while retaining the advantages of a potential flow. The application to the flow near the trailing edge of a lifting aerofoil is given

Key words: *flow, vortices, wakes*

Use of a single vortex sheet to replace a solid boundary in an incompressible flow was introduced in 1858 by Helmholtz. (The subsequent history is well documented, for example by Giacomelli[1], but some features are repeated here for coherence). In a later paper, Helmholtz in 1868 introduced ideas of the behaviour of vorticity and these were widely developed by succeeding authors culminating in the well known descriptions of Kelvin and Beltrami.

Helmholtz was trying to describe a real flow by forcing it into the framework of simple irrotational flow. He pointed out that there was nothing inherent in the theory of irrotational flow that prevented the introduction of a discontinuity in the form of a vortex sheet. He took it as obvious that the pressure field and the normal component of velocity should be continuous across a vortex sheet. This led to the requirement that his vortex sheets must lie on streamlines.

In the absence of external forces a vortex sheet in an irrotational flow is required to travel with the flow. In a real flow we know that such external forces are obtained from the effects of viscosity in regions which, following Prandtl, we call boundary layers and wakes.

Helmholtz saw that there was something different about the vortex sheets used to describe a solid boundary from those which were required to follow the simple laws of irrotational flow. The former sheets have therefore come to be called bound sheets.

The next development of the use of vortex sheets was when Lanchester first introduced his ideas of vortical layers curling up at wing tips. These ideas were later quantified by Prandtl and others and led to what is now generally known as the Prandtl–Lanchester lifting line theory of induced drag (or according to purists, lifting surface theory).

In his early paper of 1911, Prandtl appears to be quite clear that all of the vorticity could be assumed to be confined to the boundary layers and wakes. Seven years later, however, he produced another classical paper in which he presented the behaviour of the vorticity as the viscosity tends to zero. This reduced the vorticity to a single vortex sheet and greatly simplified the analytical treatment but hides the fact that vorticity is distributed over a finite thickness in a real flow.

From the point of view presented here the great success of induced drag theory in the hands of people like Betz, Munk and Glauert in producing useful irrotational flow models of the real flow is somewhat unfortunate. Some modern text books even go so far as to say that induced drag is a purely potential flow effect. A more useful description would be that it models the changes to the potential flow produced by the change of distribution of vorticity. This vorticity was generated by viscous effects in the boundary layers and near wakes, and is confined to those regions.

Vorticity distribution in a boundary layer

Lighthill[2] has presented a valuable description of the distribution of vorticity within a boundary layer. He has shown that in a two-dimensional flow, at the level of the boundary layer approximation, the only component of vorticity present is represented by vortex lines normal to the streamlines and parallel to the wall. This is the component $\zeta = \partial u/\partial y$ where

* University of Tasmania, Department of Engineering, 252C Hobart, Tasmania 7001, Australia
Received 20 October 1981 and accepted for publication on 19 February 1982

 0142–727X/82/020081–09$03.00

u is the local velocity in the direction of x along the wall and y is in the direction normal to the wall.

Lighthill then showed quite simply that the sum of all the vorticity at any section at any instant is equal to U, the free stream velocity, that its mean velocity of transport is $U/2$ and its centroid is at a distance from the wall equal to δ_1, the mass flux deficiency thickness or displacement thickness of von Karman.

New vorticity is created at the solid surface in accelerating flow. In the regions very close to the wall the velocities are always very small so the transport of vorticity through these regions is almost entirely by viscous diffusion alone. Further away from the wall the convective terms also contribute to the vorticity transport. This means that at the level of the boundary layer approximation the distribution of vorticity in a steady laminar boundary layer is described by the differential equation:

$$u\,\partial\zeta/\partial x + v\,\partial\zeta/\partial y = \nu\,\partial^2\zeta/\partial y^2$$

When this differential equation is translated in terms of vortex sheets it is seen to be equivalent to replacing the single vortex sheets used by Helmholtz and Prandtl by an infinite number of vortex sheets of infinitesimal strength distributed over a boundary layer. All of these sheets must be considered as bound because there are viscous forces which restrain them from moving with the flow in the way that Helmholtz described for his sheets.

Lighthill showed that a simple description of a boundary layer, useful for many purposes, is obtained by replacing all this vorticity by a single sheet at its centroid, that is at a distance from the wall equal to the displacement thickness. This model, however, is not always sufficient to give a useful description of the flow. This is particularly so when the Reynolds number is low enough for the boundary layers to be no longer thin in the usual sense, or when there is early separation on the suction surface. Also, when the lift force is appreciable, the resulting strong circulation provides appreciable velocity gradients in the irrotational flow outside the boundary layers and wake near the trailing edge. The usual definitions of mass and momentum flux deficiency thicknesses, which depend on the free stream velocity distribution being nearly constant, then lead to appreciable errors.

Fig 1 shows a measured velocity distribution in a wake near the trailing edge to illustrate the problem. The circled points are values measured by a hot wire anemometer and the solid line the velocity distribution calculated for a wholly irrotational flow. There is obvious difficulty in distinguishing the effect of viscosity. Further details about these measurements are postponed till later.

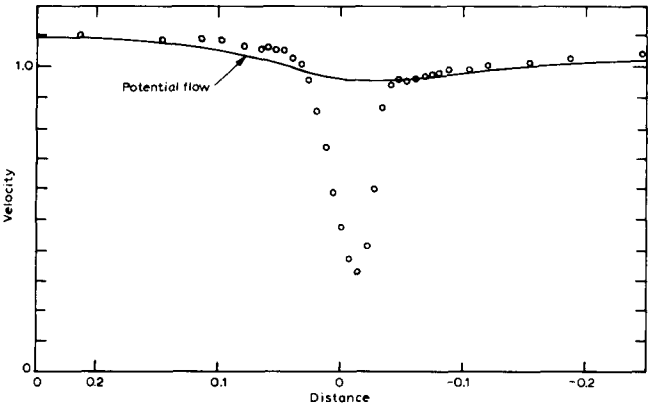

Fig 1 Velocities measured at Station 5 of Fig 14 compared with values calculated for purely potential flow (solid line)

Another difficulty with the viscous trailing edge problem is that the Kutta–Joukowsky hypothesis, that the flow near the trailing edge should be smooth, no longer leads to a simple location of the trailing edge stagnation point. The viscous forces effectively round the trailing edge. The single vortex sheet model is of little help in this regard because it does not model the momentum deficiency of the viscous regions.

The extended Kutta–Joukowsky hypothesis must include the fact that the boundary layer separates from each of the two surfaces near the trailing edge. The viscous shear layers must merge smoothly (at least in the mean flow) like reversed or suction jets enclosing recirculating regions which in most cases are small, and have small velocities.

The lack of any momentum deficiency in the single vortex sheet model is, then, a considerable handicap.

Double vortex sheet model of a boundary layer

Because a single vortex sheet model has not enough free parameters to model both mass and momentum flux deficiency the author[3] introduced a double vortex sheet model. Both sheets must be considered as bound because neither behaves like a free vortex sheet in a simple irrotational flow. Their positions

Notation

H	Boundary layer shape factor (δ_1/δ_2)
h_1, h_2	Distances from middle of wake to vortex sheets
U	Free stream velocity
u'	$(U-u)/U$ velocity deficiency ratio at middle of wake
u	Component of local velocity in direction of U
v	Component of local velocity normal to U
x	Distance in direction of U
y	Distance normal to U
δ_1	Displacement thickness
δ_2	Momentum thickness
ν	Kinematic viscosity
ψ	Stream function
ζ	Vorticity component normal to $U(\partial u/\partial y)$

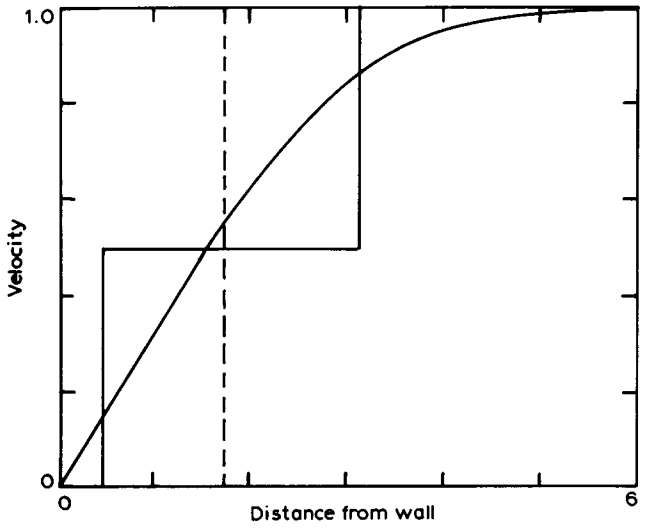

Fig 2 Comparison of velocity distributions for single vortex sheet (broken line), double vortex sheet (rectangles) and zero pressure gradient laminar boundary layer (Blasius)

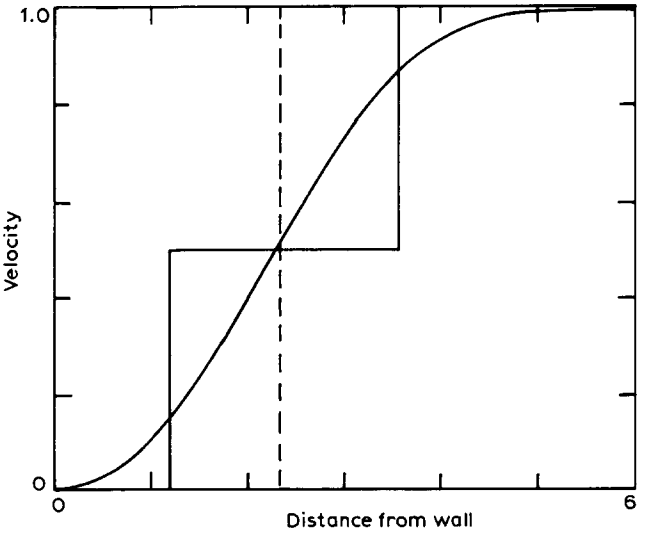

Fig 3 Comparison of velocity distributions for single vortex sheet (broken line) double vortex sheet (rectangles) and zero wall shear stress laminar boundary layer (Hartree)

are determined by the distribution of vorticity within the viscous regions.

Two vortex sheets define a potential function as soon as their positions and strength have been defined so the solutions retain all the simplicity of the linear differential equations. Within the viscous regions of the real flow the resulting irrotational flow is only a fiction to model the two most useful parameters of that flow. One must never lose sight of the viscous effects which, in the real flow, transfer vorticity from one sheet to the other and determine their location.

Two vortex sheets allow four free parameters in the values of the position and strength of each sheet. The three restrictions, that the total vorticity in a two-dimensional boundary layer equals the free stream velocity and that the mass and momentum fluxes of the double vortex sheet model should be the same as the real flow, leave one parameter still free.

The author has made a number of unsuccessful attempts to make some use of this free parameter such as placing the inner vortex sheet at the physical boundary, modelling the energy deficiency thickness of the viscous region and placing each sheet at the centroid of half the total vorticity. The arbitrariness has been resolved by placing half the vorticity in each sheet. This means that each sheet represents a step change in velocity equal to half the free stream velocity, U.

The velocity of transport of vorticity along the inner sheet is then equal to $U/4$ and that along the outer sheet is $3U/4$ so that the mean transport velocity is $U/2$ as in Lighthill's model. In addition, vorticity is diffused by viscosity in laminar flow or by turbulent eddies from one sheet to the other to preserve the requirement that the total vorticity at any section at any instant in a two-dimensional flow remain at U. These conditions are supplied externally to the simple potential flow by the viscous effects.

Two vortex sheets, each of strength $U/2$, placed two momentum thicknesses on either side of a line displaced from the wall by the displacement thickness, model a flow with the same mass and momentum flux as the real flow in regions where these thicknesses can be defined in the classical way.

The performance of this model in describing the most useful properties of the zero pressure gradient laminar boundary layer solution of Blasius is shown in Fig 2, and the comparison with the zero wall shear stress laminar layer of Hartree in Fig 3.

A typical turbulent boundary layer with H of the order of 1.5–1.6 requires the inner vortex sheet to be placed inside the solid boundary. This fact is not important so long as the model describes the mass and momentum fluxes of the real flow and has the same velocity distribution outside the viscous regions as the real flow.

It turns out, in numerical computation, that the velocity distributions calculated for regions outside the vortex sheets are very sensitive to their positions and strength. This means that the accuracy of the model can be stringently tested against measurements outside turbulent boundary layers. The usual hot wire measurements within the regions of strongly fluctuating flow are always suspect because of the uncertain effects of the fluctuations.

In the vicinity of the aerofoil, the inner sheet brings the velocity to zero just inside it, so it lies on a streamline of zero velocity. Where we can put $\psi = 0$ on this streamline the value of the stream function on the outer sheet is equal to $2U\delta_2$ so that not only is it bound but it must also be porous. Some fluid must be permitted to cross it and, in doing so, have its velocity halved so that the momentum flux of the model accurately replaces that of the real flow including the viscous effects.

Any conclusions about the detail of the real flow in the region between the two vortex sheets is therefore likely to be subject to serious error. In particular, any statements about the energy of this part of the flow are prone to be misleading.

Double vortex sheet model of a wake

In the near wake of a lifting aerofoil the effect of circulation is to introduce velocity gradients in the real irrotational flow outside the viscous wake. The effect of these gradients, as shown in Fig 1, is that the classical definitions of displacement and momentum thicknesses are misleading when applied to measured values. Published values of these parameters in this region must therefore be used with caution. In particular, the frequently published statement that there is always a discontinuity in the displacement thickness at the trailing edge is obviously incorrect.

Further downstream, at a distance which depends on the value of the lift, the extent of the separated region or the blade spacing for a cascade of aerofoils (so that no general rules can be given), the distributions of pressure across the flow and velocity outside the wake become nearly uniform. Under these conditions the usual definitions for displacement and momentum thicknesses can be applied to a blade wake. It is fairly obvious that two equal vortex sheets can have their positions and strengths defined in such a way as to model the mass and momentum fluxes of the far wake.

It appears conceptually simpler, however, to continue the two vortex sheets from the boundary layers on each side of the aerofoil into the wake and to use four vortex sheets to describe a far wake. The vorticity in each half of the wake is then equal to the difference between the free stream velocity and that in the middle of the wake. The process of wake decay appears as a transfer of vorticity from one side to the other where it is cancelled by vorticity of opposite sign. This is, of course, the well known Taylor model of vorticity transfer in a turbulent boundary layer extended into the wake. In the less common situation of a laminar wake the mechanism of transfer of vorticity is that of diffusion by viscosity and the rate of decay of the wake is much slower.

When the arbitrary decision is made to put half of all of the vorticity in each side of the wake into each of the two vortex sheets which describe it and the von Karman definitions of displacement and momentum thicknesses can be applied with sufficient accuracy, it is easy to show that the distances of the vortex sheets from the middle of the wake are given by:

$$\tfrac{1}{2}u'h_1/\delta_2 = [(1-\tfrac{1}{2}u')H - 1]/u'$$

and

$$\tfrac{1}{2}u'h_2/\delta_2 = H - \tfrac{1}{2}u'h_1/\delta_2$$

in which h_1 and h_2 are the respective distances of the two sheets from the middle of the wake and u' is the non-dimensional velocity deficiency ratio.

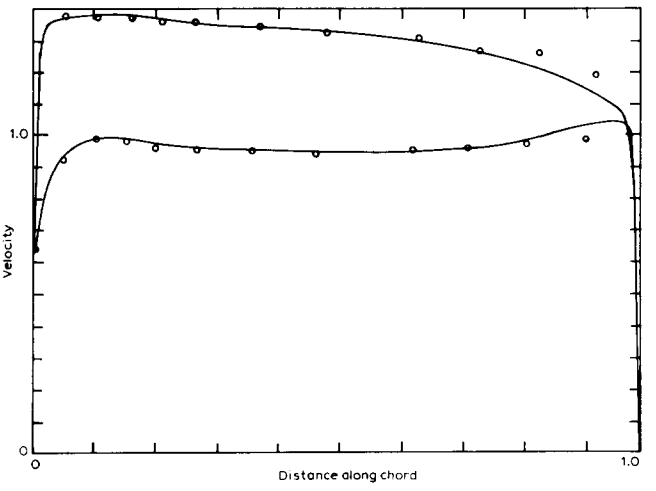

Fig 4 Velocity distribution over aerofoil from surface pressure tapping readings (circled points) compared with values calculated for purely potential flow (solid line)

Fig 13 shows four vortex sheets and the corresponding velocity distribution for comparison with measured velocities (circled points). The measuring station was one half chord length from the trailing edge of the aerofoil whose near wake is shown in Fig 1.

Each of the four vortex sheets used to describe a wake is bound to the others in the sense that the relative positions and strengths are determined by the viscous effects. In order to model these effects by the potential function defined by the vortex sheets they must be permitted to break the Helmholtz rules for free sheets. None of the sheets in a wake is on a streamline so each must be regarded as porous in the same sort of way as the outer sheet that forms part of the model of a boundary layer on an aerofoil.

A wake of an aerofoil in steady flow is a region of velocity deficiency (relative to the aerofoil) and is carried along with the irrotational flow outside it. The Reynolds stresses are usually small except close to the aerofoil and so the wake is usually subject to nearly the same pressure field as the irrotational flow. Any downstream body which perturbs the pressure field adds a contribution to the spread of the wake and this effect must appear in the positions and strengths of the sheets that model it together with the viscous (including turbulent) effects.

So long as turbulent eddies persist in entraining fluid from outside the wake, new vorticity in the mean flow is being generated by stretching and turning of vortex lines of the instantaneous flow in the manner discussed by Lighthill[2]. This effect appears as a mixing loss and accounts for an increase in momentum thickness of the wake as it recedes from the aerofoil, and an increase in the gaps between the sheets.

Flow near a trailing edge

The advantage of the double vortex sheet model over the ordinary boundary layer analysis is that it is not restricted to nearly plane flow. The two sheets can

Table 1 Axial location of measuring stations

Station number	Position	Fig
1	0.833	5
2	0.900	6
3	0.967	7
4	1.021	8
5	1.042	9
6	1.076	10
7	1.167	11
8	1.333	12
9	1.500	13

be continued through regions of separated or strongly curved flow to provide a simplified quantitative description of the real flow in regions where the ordinary boundary layer parameters cease to be useful.

When the sheets are properly located with the correct strength they define a potential function which describes a flow with essentially the same mass flux and momentum flux at any section as the measured flow. When the flow is strongly curved, the whole of the momentum is not modelled exactly because the velocity directions at different parts differ between model and real flow.

Fig 9 shows a velocity traverse calculated from a double vortex sheet model compared with the measured values (circled) of Fig 1 (details of the model and its use in calculation are given later).

This traverse was very close (about 1 mm downstream) to the position of the downstream stagnation point in the mean flow. Within the viscous region the velocity fluctuations were of the order of twenty percent of the free stream velocity. Under these conditions, the accuracy of the measurements is suspect and the agreement between the measured and modelled values must be regarded as a satisfactory indication that the sheets have been properly located. It is thought that the differences between the two sets of values outside the viscous region are significant even though they are only of the order of the expected errors in measurement. A closer fit can always be obtained by more attention to the details of location of the sheets and their strengths but, in this case, it was felt that the accuracy of the overall description of the whole flow was as high as warranted by the precision of the measurements. The point is made here mainly to reinforce the earlier statement that velocities calculated from the model for regions outside the viscous regions help greatly in determining the precision of location of the vortex sheets.

The double vortex sheet model thus gives a quantitative description of the important integral properties of the flow with useful precision in a simple model. The usefulness of the boundary layer concept is considerably extended to regions where the usual integral parameters of displacement and momentum thickness cannot be calculated with any useful accuracy. The whole flow pattern around an aerofoil can now be described much more precisely than hitherto possible by simple means.

Description of the aerofoil

The aerofoil whose flow pattern is presented here is actually a section at mid blade height of the inlet guide vanes of an experimental axial flow compressor. It is the property of the Aeronautical Research Laboratories (an Australian government agency) and has been operated extra-murally at the University of Tasmania for over twenty years. Details of the compressor have been published elsewhere[4] and are only incidental here.

The shape is that of the British C4 section with a circular arc camber line having 27.5° camber, operating at zero incidence with a space/chord ratio near unity to turn the flow through nearly 22°. The chord length is nearly 76 mm.

This aerofoil was conservatively designed and has the quite moderate lift coefficient of 0.8 with a Reynolds number based on chord length and vector mean velocity through the cascade of nearly 100 000. Also, boundary layer growth on the annulus walls of the compressor causes the axial velocity to accelerate to about 3% higher as the flow passes through the blade row. Despite these facts, which are expected to be favourable to boundary layer development, there are some surprising features of the flow which make it useful to illustrate the application of the double vortex sheet model.

The velocity distribution over the aerofoil (non-dimensionalised with respect to vector mean velocity) is shown in Fig 4. The circled points are values calculated from pressure tappings on the blade surface. The solid line gives values calculated by the two-dimensional potential flow method of Martensen[5] with some modifications along the lines suggested by Hess and Smith[6]. This method of calculation replaces the aerofoil with a single vortex sheet at its surface, and uses the condition that the velocity component at the sheet (but just inside it) in the direction parallel to the surface is zero.

The trailing edge of the C4 section is rounded as shown in Fig 14, so the position of the trailing edge stagnation point cannot be determined by the simple Kutta–Joukowsky condition. Its position was determined for the results presented in Fig 4 by the condition that the angle of turning of the calculated flow should equal the measured value.

The agreement between the calculated and measured values indicates that the flow over most of the aerofoil was predominantly two-dimensional. There are the usual discrepancies near the trailing edge which are customarily dismissed as being due to viscous effects not properly understood. It is one purpose of this paper to elucidate these effects.

Hot wire measurements

A number of velocity traverses in the circumferential direction through the boundary layers on the blade and through the near wake were made with standard DISA constant temperature anemometer equipment. The axial location of the hot wire was accurately measured by a cathetometer mounted outside the fan and looking through a Perspex window. The wire was held fixed and the whole blade row rotated to vary the circumferential position.

Nine of these traverses are reported here. Their locations in the axial direction of the fan are shown in Fig 14 and in Table 1. These are presented as axial distances from the leading edge expressed as fractions of the length of the blade chord projected onto an axial plane.

The clear spacing between blade rows is about one chord length. Station 9 was about half a rotor blade spacing upstream of the rotor leading edges and so was clear of unsteady effects from the moving row of blades, yet far enough downstream of the inlet guide blade row for the free stream velocity to be nearly uniform, as shown in Fig 13.

Mean velocities were obtained from an integrating voltmeter compared with a calibration curve smoothed by fitting a parabola to a modified King's law, using Nusselt number varying as the 0.45 power of Reynolds number as the first approximation. This procedure has been found to give more consistent results than using the simple King's law on its own, particularly when comparing measurements made over a large range of atmospheric conditions.

At each measuring point the hot wire anemometer voltage signals were also passed through a lineariser and displayed on an oscilloscope to observe the unsteady effects. Comments on these will appear where they affect the results presented.

Positions and strengths of vortex sheets

The boundary layers over most of the surface were known to be laminar from china-clay visualisation studies while the agreement between the velocity distribution from the simple potential flow calculation and the pressure measurements shown in Fig 4 indicated that there were no gross errors in the latter. These were accordingly used with the Thwaites method to estimate the boundary layer development and the positions and strengths of the vortex sheets to replace the viscous regions up to separation. This occurs right at the trailing edge on the pressure surface and at about 67% chord on the suction surface as shown on Fig 14 and partially confirmed by china-clay tests. The velocities obtained from the pressure measurements do not allow a prediction of the point of separation because the effects of separation are already included in the pressures so the potential flow calculation was used for this purpose.

A preliminary estimate of the positions and strengths of the vortex sheets was obtained from some rough calculations on the measured velocity traverses. These were then plotted on an axial section as in Fig 14 and the data smoothed in this plane by drawing mean straight lines over most of the field. The strengths of the vortex sheets fell near a straight line when their squares were plotted against axial distance so an average line was taken.

The vortex sheets were divided into segments over which the strength was taken as constant and velocity distributions calculated by simply summing the contributions from all the segments and the vector mean velocity. This gave a useful preliminary picture of the whole flow pattern.

A number of adjustments to the measurements were then made to allow for effects which became apparent. Near the trailing edge on both surfaces the velocities obtained from hot wire readings were up to 3% higher than those inferred from the pressure tapping readings. The difference was attributed to Reynolds stresses and the hot wire values were adopted as correct.

An earlier (unpublished) traverse with a yawmeter over the whole flow area at Station 9 had shown that the axial velocity was 3% higher at this station than upstream of the blade row. It was assumed that this was a measure of the contribution of vortex sheets on other surfaces to the flow at this station. This amount was subtracted from the measured values as a correction for the three-dimensional flow effects. At other stations which crossed the wake similar corrections were made. The measured values were reduced by up to the same amount at a few points near the middle of the flow passage between blade wakes to fit them to the two-dimensional calculations. No such corrections were made to traverses over the blades themselves on the grounds that they were already included in the measured velocities.

Another set of velocity calculations was made and the positions of the vortex sheets adjusted to make the integral of the velocity and its square over the viscous region the same as that obtained from the measured values. This is not quite the same as equating mass and momentum fluxes because the flow angles must be different from model to real flow. The error from this source appears to be no greater than expected errors of measurement.

The shift of position of the vortex sheets was accompanied by a corresponding shift in their strengths. The suction surface side of the wake was almost fully turbulent from the time that it left the trailing edge and the strengths of the sheets on this side were fitted to a square root decay law. The boundary layer on the pressure side was still laminar at separation and commenced transition to turbulence near Station 4 so the rate of decay of sheet strength was initially faster there and asymptotic to the same square root decay law as the suction side, reaching it somewhere between Stations 6 and 7.

A number of repetitions of measured traverses at Stations 7 and 8 as well as others not reported here had indicated that the measurement of the wake position could not be repeated to closer than 1 mm. The expected accuracy of location by the two vortex sheet model is rather higher so it appears that the flow pattern does not repeat itself closer than this. Such variations are not unexpected with the large regions of strongly separated flow shown on Fig 14. The whole wake measurements have been moved about 1 mm towards the pressure side at Station 7 in order to bring the vortex sheets onto straight lines.

The positions of the vortex sheets at the various traverses are then as shown in Fig 14 and the resulting velocity calculations compared with the measurements on the other figures. The accuracy of the measurements limits the advantages to be gained by any further adjustment and a useful description of the flow has already been obtained.

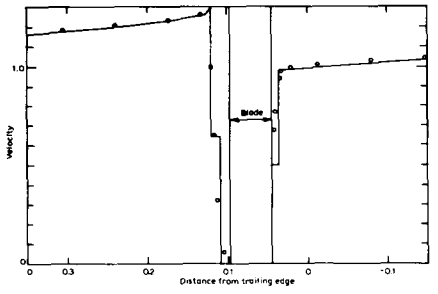

Fig 5 Velocities measured near aerofoil at Station 1 of Fig 14 (x/c = 0.833) compared with values calculated from double vortex sheet model

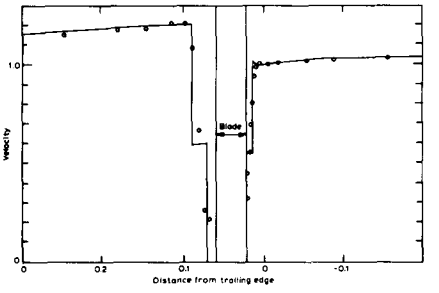

Fig 6 Velocities measured over aerofoil at Station 2 of Fig 14 (x/c = 0.9) compared with values calculated from double vortex sheet model

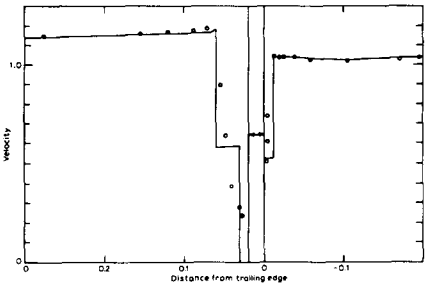

Fig 7 Velocities measured near aerofoil at Station 3 of Fig 14 (x/c = 0.967) compared with values calculated from double vortex sheet model

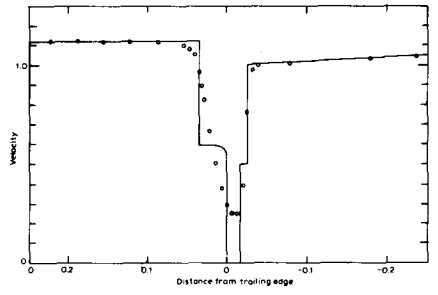

Fig 8 Velocities measured in near wake at Station 4 of Fig 14 (x/c = 1.021) compared with values calculated from double vortex sheet model

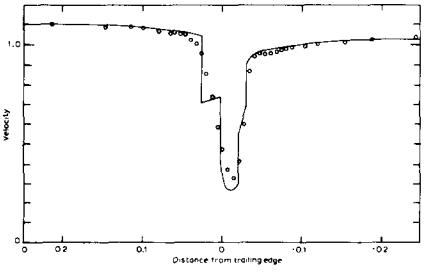

Fig 9 Velocities measured in wake at Station 5 of Fig 14 (x/c = 1.042) compared with values calculated from double vortex sheet model

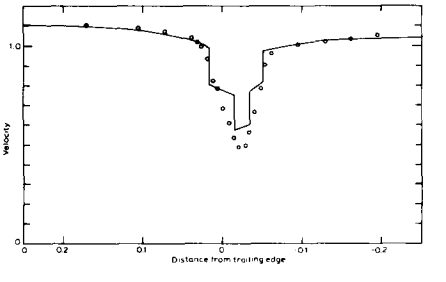

Fig 10 Velocities measured in wake at Station 6 of Fig 14 (x/c = 1.076) compared with values calculated from double vortex sheet model

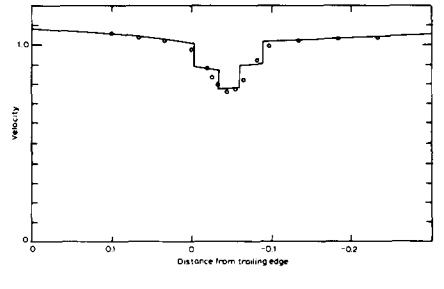

Fig 11 Velocities measured in wake at Station 7 of Fig 14 (x/c = 1.167) compared with values calculated from double vortex sheet model

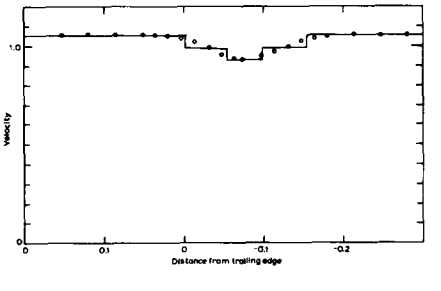

Fig 12 Velocities measured in wake at Station 8 of Fig 14 (x/c = 1.333) compared with values calculated from double vortex sheet model

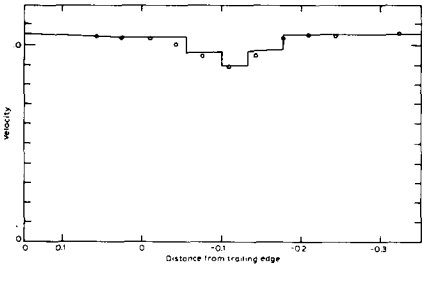

Fig 13 Comparison of velocities measured at Station 9 of Fig 14 (x/c = 1.5) with double vortex sheet model

Description of flow

The boundary layer on the pressure side reaches the laminar instability condition near the peak of velocity at about 10% of chord as shown in Fig 4. The resulting Schlichting–Tollmien waves must grow quite rapidly during the ensuing deceleration to about mid chord and then become stabilised as growing inertial waves over the last 25% of chord where the flow accelerates. These inertial waves have strong three-dimensional components and are sometimes almost missed by short hot wire probes whilst at other times the fluctuating component as seen on the oscillograph is as much as 30% of the free stream velocity.

A strong whistle is always heard with a stethoscope in the region of Station 3 at a frequency corresponding to the neutral equilibrium condition of the local boundary layer. The Reynolds stress associated with these waves causes the free stream velocity to be higher than that inferred from the local pressure tapping. The local velocities measured by the hot wire outside the viscous regions shown in Figs 5, 6 and 7 are closer to the potential flow values shown in Fig 4 than they are to those calculated from pressure tapping readings.

The measured boundary layers on the pressure side in Figs 5, 6 and 7 appear to be thinner than indicated by the vortex sheets (whose position has been calculated by the Thwaites method) largely because no allowance has been made for wall correction to measurements in these thin layers. There is plenty of other evidence to indicate the reliability of the Thwaites method without trying to justify it here.

Separation on the pressure side occurs very soon after the flow rounds the trailing edge. The location of the vortex sheets in Fig 14 indicate that the flow turns through nearly 20° before separation. This is a much greater turning than one would associate with a laminar boundary layer, the difference being attributed to the mixing effect of the large inertial waves.

The boundary layer on the suction side is predicted to separate (as has already been described) at about 67% chord. Fig 14 shows separation to be smooth rather as though the wall curves away from the flow than vice versa.

The separated laminar shear layer continues to diffuse vorticity as shown in Fig 14 by the small spread in the gap between the vortex sheets. The velocity distribution shown in Fig 4 indicates that while the separated shear layer remains predominantly laminar the velocity gradient outside the layer is nearly zero. The simple momentum integral equation requires some change in velocity corresponding to the diffusion of vorticity but this is small and probably overshadowed by the Reynolds stresses from inertial waves under these conditions.

The onset of transition to turbulence is predicted by the method of Walker[7] to occur at 81% chord, just upstream of Station 1. A quite rapid change of conditions is indicated at about this position by the velocities inferred from pressure tapping readings as shown on Fig 4 and by the positions of the vortex sheets shown on Fig 14.

The velocity distribution shown in Fig 5 for Section 1 is that of a well separated shear layer. The local kink in the calculated velocity just outside the outer shear layer on the left hand or suction side appears to be part of the limitations of the model and due to insufficient detail in the modelling of the vortex sheets for the numerical calculations. Other similar local kinks appear in the following figures as errors in numerical modelling but that in Fig 7 for Station 3 appears to reflect some of the properties of the real flow.

Reference to Figs 6 and 7 shows that the shear flow remains separated over the whole downstream third of the blade chord and the turbulence level increases over the last twenty per cent of chord. It can be seen in Fig 14 that the outer vortex sheet stays close to a straight line as the turbulence grows while the inner sheet curves around towards the aerofoil surface.

Station 4 is taken to be upstream of the trailing edge stagnation point because many of the linearised hot wire signals went to zero with the characteristic spike on the oscilloscope that accompanies a reversal of flow. The same sort of evidence indicated that Station 5 was downstream of the stagnation point. The flow is always highly unsteady in these regions with strong fluctuations from inertial waves in the laminar flow on the pressure side as well as from the turbulent flow from the suction side, so that the precision of the linearised velocity measurements is expected to be low. The exact location of the trailing edge stagnation point is therefore doubtful but it is no longer very significant when the flow can be so well described by continuing the vortex sheets which describe the boundary layers into the wake.

At Station 5 shown on Fig 9 the shear layer starts to go turbulent. Transition is much shorter here than on the relatively quiet suction side, partly because the inertial waves had become so large and partly because of the effect of turbulent eddies from the suction side boundary layer. Fig 14 shows the very rapid growth of the gap between the vortex sheets just downstream of the stagnation point.

The two separated boundary layers join like two negative or suction jets and are turned in proportion to their strengths.

There appears from Fig 9 to be an appreciable net shear force across the wake arising from the much greater level of turbulence on the suction side producing higher Reynolds stresses there. These wakes are too thin to allow useful measurements of Reynolds stresses even with short wires; the overall length covering the four vortex sheets of Fig 9 is less than 5 mm.

It is clear from Fig 9 that an excess of vorticity must be shed into the wake from the suction side, amounting to over 10% of the velocity on that side in this case. The lift-circulation theorem is in error by nearly the same amount, because it ignores the net shear force and the changes in static pressure associated with the Reynolds stresses and their resultants. Proofs that no excess of vorticity can be fed into a wake ignore these effects. Admittedly, the behaviour of the shear layers on this aerofoil appear to be rather extreme and, if it had been known, would

have been avoided by using a slight reflex on the camber line over the last third of chord. Nevertheless, it is a quite conservative design by conventional methods. The massive separation of the flow was most unexpected and not revealed until the double vortex sheet model was applied.

Downstream of Station 7 shown in Fig 10 the behaviour of the wake is pretty much as that of other wakes recorded in the literature, except for the small excess in vorticity which was initially attributed to the unsteadiness of the flow, experimental error and to three dimensional effects. It was not until several years after the initial concept of the double vortex sheet model that it was possible to present the simplified description of the flow which has been discussed above.

Caution must be observed in applying the quantitative results obtained here to two dimensional flow. These results have been obtained from within a machine where there is a strong radial pressure gradient in the direction normal to the plane of Fig 14. Cross flows within the separated regions and wakes mean that some of the vorticity shown in the measured velocity distributions was generated outside the radius of this section and convected inwards.

Concluding remarks

The double vortex sheet model is not limited to two dimensional flow any more than the single vortex sheet model. Streamwise components added to the vorticity vectors of one sheet combined with similar ones of opposite hand on the other sheet model a cross flow. Only one free parameter is left so it is not possible to model the whole mass and momentum flux deficiencies of the viscous region. Grainger[8] has pointed out that for small cross flows there is enough freedom to be obtained by relaxing the requirement that the sheets should have the same strength in the direction normal to the streamwise direction. Realistic descriptions of large cross flows in which the direction reverses requires the addition of another pair of sheets. Useful models of other flow patterns can be obtained by adding single vortex lines as in the grossly simplified tip vortex model.

This approach lends itself to the successive Goldstein approximations. The wholly potential flow calculation of velocity presented in Fig 4 enables initial estimates of the positions of the various vortex sheets. These are similar to those presented here as having been calculated from measured velocities. The conditions that the inner vortex sheet

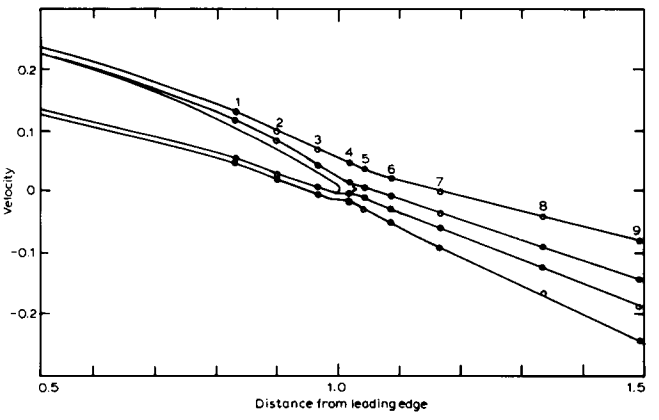

Fig 14 Section through vortex sheets in direction of flow

over the aerofoil is a streamline and that the four vortex sheets of a wake can define a stagnation streamline are sufficient to define the velocities for a given vector mean velocity. There is very little more difficulty in setting up Martensen's equations[5] when two sheets are used per side than one. The difficulty arises in replacing the Kutta condition. We need more information about the Reynolds stresses which define the excess of vorticity to be fed into the wake.

References

1. **Giacomelli R.** in *Aerodynamic Theory, Vol I,* ed *W. F. Durand, (Dover 1934)*
2. **Lighthill M. J.** in *Laminar Boundary Layers, ed L. Rosenhead (Oxford University Press, 1963)*
3. **Oliver A. R.** Definition of Wakes by Vortex Sheets. *Proc. Fourth Aus. Conf. on Hyd. and Fluid Mech. Melbourne, 1971*
4. **Oliver A. R.** Comparison between Sand Cast and Machined Blades in the Vortex Wind Tunnel. *Report ARL/ME 103, 1961, Aero. Res. Labs., Melbourne, Australia*
5. **Martensen E.** Berechung der Druckwerteilung an Gitter-Profilen in ebener Potential Stromung mit einer Fredholmschen Integralgleichung. *Arch. Rat. Mech. und Anal, 1959 3,*
6. **Hess J. I. and Smith A. M. O.** Calculation of Potential Flow about Arbitrary Bodies. *Prog. in Aero Science, 1967*
7. **Walker G. J.** An Investigation of Boundary Layer Transition on an Axial-Flow Compressor Blade. *Report ARL/ME 122 Aero. Res. Labs., Melbourne, Australia, 1968*
8. **Grainger C. F.** Personal communication, *1974*